



## Research Article

# A Fast Global Optimal Strategy for Iteration Closest Point Using 2D-BnB and Its Application to Rail Profile Registration

Dingfei Jin <sup>1,2,3</sup> and Hua Ma <sup>4</sup>

<sup>1</sup>Key Laboratory of Intelligent Computing and Information Processing of Ministry of Education, Xiangtan University, Xiangtan 411105, China

<sup>2</sup>School of Automation and Electronic Information, Xiangtan University, Xiangtan 411105, China

<sup>3</sup>SGSG Science & Technology Co. Ltd. Zhuhai, Zhuhai 519085, China

<sup>4</sup>High Speed Railway Operation and Maintenance Engineering Research Center of Henan Province, Zhengzhou 450000, China

Correspondence should be addressed to Hua Ma; [rosyhorse@126.com](mailto:rosyhorse@126.com)

Received 22 September 2023; Revised 6 November 2023; Accepted 30 November 2023; Published 14 December 2023

Academic Editor: Rajkishor Kumar

Copyright © 2023 Dingfei Jin and Hua Ma. This is an open access article distributed under the Creative Commons Attribution License, which permits unrestricted use, distribution, and reproduction in any medium, provided the original work is properly cited.

Profile registration is critical to rail wear measurement with line structured light, and the most popular registration method is iteration closest point (ICP). Unfortunately, ICP is often invalid in actual applications because it is easy to trap into local minima. To solve this problem, we propose a hybrid 2D-point-set registration method which combined ICP to branch and bound. In this way, we can ensure that the ICP algorithm converges to the global optimum. This strategy can achieve high-registration precision, but it suffers from large computation costs. To address this issue, we propose an acceleration scheme by sparsely sampling the point-set before registration to relieve computation burden. Extensive experiments are conducted to verify the precision, stability, and efficiency of our method. The results show that our method has superior precision and stability compared to the other typical profile registration methods. The ability to achieve fast registration speed which is suitable for dynamic measurement is another contribution of our work.

## 1. Introduction

In this study, we work on seeking a fast and high-precision profile registration method for rail wear measurement. Wear measurement is one of the most important tasks of routine track quality inspection [1, 2]. The measurement results, reflecting the rail section geometry, can be aligned with the standard profile to obtain the wear information of the rail [3, 4] and can provide details for the routine maintenance.

With the advantages of high precision and low cost, line structured light (LSL) has become one of the most popular methods for rail wear measurement [5, 6]. As shown in Figure 1(a) [7], the wear measurement system with LSL is mainly composed of a line laser and a digital camera.

When measuring the rail profile, the system captures the laser strip projected onto the surface of the rail through the camera. Then the coordinates of laser strip in Figure 1(b) can be calculated out easily. Utilizing these coordinates, we can get the measured profile, and align it with the standard rail

profile to calculate wear [8], which is shown in Figure 2, where  $r$  denotes rotation angle, and  $[t_1, t_2]^T$  denotes translation vector. LSL is used to acquire the rail profile, and the process of aligning the measured rail profile to the standard profile is called profile registration [9].

The key aspect to rail profile registration are precision and efficiency, and iteration closest point (ICP) [10] is the preferred method for the registration problems. However, the precision of ICP is unstable because it is easy to trap to minima. To address this issue, we attempt to seek a global optimal registration algorithm for ICP on the planar space in this paper. In  $SE(2)$  space, ICP is first used to obtain a local optimal solution, and then branch and bound (BnB) is used to search for a solution with an error smaller than ICP. Finally, these two steps are alternately executed until the global optimal solution is found. In addition, to satisfy the efficiency requirements of dynamic measurement for the rail, we propose an acceleration strategy via sparse sampling for this

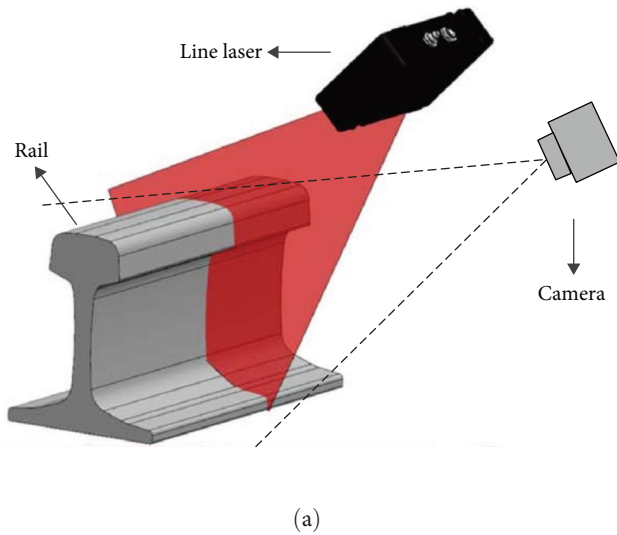


FIGURE 1: Schematic diagram of LSL: (a) measurement device and (b) the coordinates of laser strip.

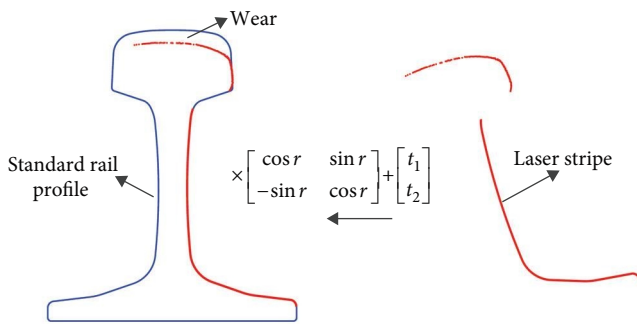
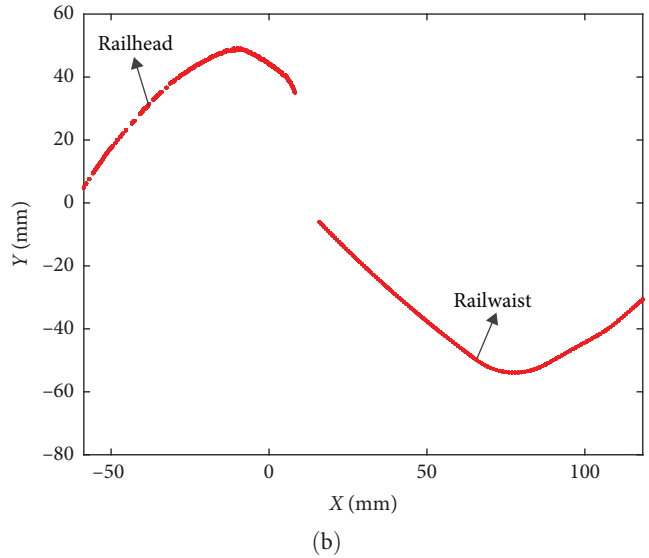


FIGURE 2: Rail profile registration.

algorithm. Thus, the rail profile measurement with LSL will be more precise and efficient.

The main contributions of this work are as follows:

- (1) In 2D space, a global optimal point-set registration algorithm is derived. In this algorithm, BnB and ICP are collaboratively used. Compared to the common global search strategies, our method finds the global optimal solution to the 2D-point-set registration problem directly.
- (2) For BnB, we derived the feasible range of parameters and the upper and lower bounds of registration error. Once a local optimal solution through ICP is acquired, BnB with given parameter range and bounds will help the algorithm find a new solution with smaller error. This can theoretically guarantee the global optimal solution
- (3) To help the above method to be more efficient and suitable for high-speed dynamic measurement, we sparsely sampled the set of points to be registered. This can obviously improve registration efficiency while ensuring precision.



- (4) Extensive experiments are conducted to verify the precision, stability, and efficiency of the proposed method. The results show that our method ensures competitive performance compared to the other similar typical registration methods.

The rest of this paper is organized as follows: Section 2 presents a brief review of related works. Section 3 illustrates the principle of rail profile registration. Section 4 introduces the details of global optimal ICP registration algorithm in planar space and its acceleration strategy. Section 5 elaborates the experiments and discussions. Conclusions and future works are drawn in Section 6.

## 2. Related Works

Profile registration directly determines the measurement precision, so it has become the research emphasis of rail profile measurement. In recent decades, there are many studies on the registration problems [12, 13], most of them take the profile to be measured and the standard model as two point-sets, and implement registration by solving the rigid transformation of them. ICP can be directly applied to point-sets without depending on the features of original data. In addition, it has concise concept and stable performance. Therefore, it is become the most popular registration algorithm in engineering practice and theoretical research for rigid transformation of point-sets [14]. Simultaneously, ICP is also the most commonly used method for rail profile registration [15, 16]. To improve the robustness and precision of ICP, Xiong et al. [17] proposed a registration method based on adaptive ICP and Kalman filtering. Yi et al. [18] proposed a sparse ICP algorithm for registration of non-worn regions of rails. Gao et al. [10] proposed a novel probability iterative closest point with normal vector algorithm for robust rail profile registration. Yang et al. [7] proposed a sparse scaling iterative closest point for rail profile inspection.

Shi et al. [19] uses KD tree to improve ICP to achieve high-precision registration.

However, these ICP-based methods are often easy to trap into local minima in actual applications. Under these circumstances, the registration result is incorrect, thus resulting in wrong registration results. There are many approaches to solve the local minima for ICP. In this paper, we roughly divide these methods into three categories: preregistration methods, global methods, and globally optimal methods.

The preregistration methods attempt to use other methods to give a rough registration result for the two point-sets. Then this result is taken as the initial value of ICP to increase the probability of it to achieve global optimization. The most frequently used preregistration methods include that feature histogram [20], shape context [21], local preserving of features [22], and minimum relative motion entropy (MRME) [23]. These methods can improve the registration accuracy of ICP evidently. However, once the initial value is estimated inappropriately, it will inevitably lead to incorrect registration results.

The global methods usually combine ICP with nature-inspired optimization algorithms [24, 25], such as particle swarm optimization [26, 27], genetic algorithm [28, 29], simulated annealing method [30, 31], discrete cat swarm optimization [32], and coati optimization algorithm [33]. These methods can make ICP to jump out local minima in a probability, but it cannot theoretically guarantee the global optimal solution. Nevertheless, it will inevitably increase the amount of calculation.

The globally optimal methods attempt to seek a reliable algorithm that can ensure the global optimum, and the BnB method [34, 35] is usually the preferred method for such schemes. Go-ICP [36] is the representative of such methods. In  $SE(3)$  space, it uses the oc-tree to subdivide the initial space into smaller subspaces, uses the BnB method to remove the unfavorable space, and continues to subdivide the space that meets the threshold conditions, thus finding the global optimal transformation. In addition, Liu et al. [37] has decoupled the translation and rotation optimization and proposed a fast BnB algorithm, which improved the algorithm efficiency. In addition, AA-ICP [38] also provides an acceleration scheme. These methods guarantee the global optimal solution for ICP theoretically. However, the complexity increases exponentially. When there are too many points in the set used for registration, it often cannot be applied in practice because of poor efficiency. These methods can theoretically find the global optimal solution for ICP. However, its complexity increases exponentially. When there are too many points in the set used for registration, it often cannot be used in engineering practice because of the slow convergence speed.

Technically, our study belongs to globally optimal methods. We attempt to seek a global optimal registration algorithm for ICP to guarantee its global optimal solution. In the following, we will design a new strategy for this issue and attempt to relieve the calculation burden. This will make this method more suitable for dynamic rail profile registration.

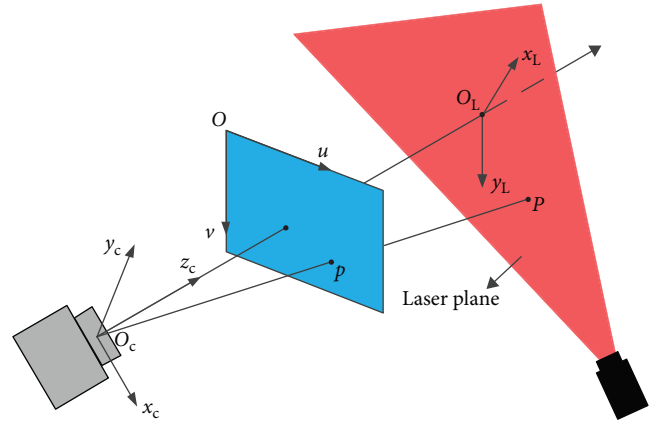


FIGURE 3: The mathematical model of LSL.

### 3. The Principle of Rail Profile Registration

In the abstract, we have briefly introduced to the concept of rail profile registration. To present this problem in detail, we first introduces the mathematical model of LSL illustrate how to acquire the coordinates of the laser stripe, and then give an supplement to the profile registration problem.

**3.1. The Mathematical Model of LSL.** As shown in Figure 3,  $O_c x_c y_c z_c$  denotes the camera coordinate system, and  $Ouv$  denotes the imaging plane coordinate system of the camera.  $O_L x_L y_L$  denotes the plane coordinate system of the laser, and its origin  $O_L$  is the intersection point between the camera optical axis  $O_c z_c$  and the laser plane.  $P$  denotes a point on the laser plane. We set its coordinate in the camera coordinate system as  $(x, y, z)^T$ , and its projection coordinates in the imaging plane coordinate system of the camera as  $(u, v)^T$ . Thus, we can get

$$\gamma \begin{bmatrix} u \\ v \\ 1 \end{bmatrix} = \mathbf{K} \begin{bmatrix} x \\ y \\ z \end{bmatrix}. \quad (1)$$

In Equation (1),  $\gamma$  denotes a nonzero constant.  $\mathbf{K}$  denotes a matrix with the size of  $3 \times 3$ , which is called the intrinsic matrix of the camera [39].

We set the equation of the laser plane in the camera coordinate system as follows:

$$ax_c + by_c + cz_c + d = 0. \quad (2)$$

In Equation (2),  $a, b, c$  and  $d$  denotes the coefficients of plane equations. [40] We can get the equation of line  $O_c P$  through Equation (1), and can obtain the coordinate of any point on the laser stripe by combining  $O_c P$  with Equation (2).

In this way, we can calculate the 3D coordinate set of the entire laser stripe. Then, we project this 3D-point set onto the laser plane to form a 2D-point-set. Thus, the 2D coordinates of the laser stripe shown in Figure 1(b) can be acquired.

In addition, to guarantee high-measurement precision, we often adopt mechanical devices to make the laser plane as strictly parallel to the rail section rail as possible.

**3.2. Rail Profile Registration.** The laser strip projected onto the surface of the rail reflects the real geometry of the rail section. After we acquired its coordinates, we can align it to the standard profile, and this process is called rail profile registration.

Usually, there is obvious wear on the railhead, but no wear on the railwaist, and we only concern the wear at the railhead. Therefore, during the registration process, we only use the waist of the measured profile and the standard profile. We denote these two railwaist profiles as  $X$  and  $Y$ , respectively. The goal of rail profile registration is to seek a suitable rotation matrix  $R$  and translation vector  $t$  to make  $X$  align to  $Y$ , i.e.:

$$RX + t \rightarrow Y, \quad (3)$$

where in Equation (3),

$$R = \begin{bmatrix} \cos r & \sin r \\ -\sin r & \cos r \end{bmatrix}, \quad (4)$$

$$t = \begin{bmatrix} t_1 \\ t_2 \end{bmatrix}. \quad (5)$$

Once the transformation from  $X$  to  $Y$  is obtained, we can easily get the wear of the railhead based on this transformation, which is shown as Figure 2.

## 4. Fast and Global Optimal ICP Algorithm for 2D Point-Set

In this section, we will discuss how to derive a globally optimal registration method for 2D-point-set  $X$  to  $Y$ , and then seek an acceleration strategy for this method.

**4.1. ICP.** ICP was first proposed in 1992 [11]. Although after more than 30 years, because of its concise concept and excellent performance, it is still the most preferred method for handling point-set registration problems. Most of the other registration methods are variants to improve the performance of ICP. In this section, we provide a brief introduction to the concept of ICP.

We set two 2D point-sets as  $X = \{x_i\}$ ,  $i = 1, 2, \dots, m$  and  $Y = \{y_j\}$ ,  $j = 1, 2, \dots, n$ . ICP can acquire a rotation matrix  $R \in SO(2)$  and translation vector  $t \in \mathbb{R}^2$  to align  $X$  to  $Y$ . For this, we first need to minimize Equation (6) as follows:

$$E = \sum_{i=1}^m e_i(\mathbf{R}, \mathbf{t})^2 = \sum_{i=1}^m \left\| \mathbf{R}x_i + \mathbf{t} - y_{j^*} \right\|^2. \quad (6)$$

In Equation (7),  $e_i(\mathbf{R}, \mathbf{t})$  denotes the residual error for  $x_i$ . Given  $(\mathbf{R}, \mathbf{t})$ , the point  $y_{j^*} \in Y$  is denoted as the optimal correspondence of  $x_i$ , which is the closest point to the

transformed  $x_i$  in  $Y$ , i.e.:

$$j^* = \operatorname{argmin}_{j \in \{1, 2, \dots, n\}} \left\| \mathbf{R}x_i + \mathbf{t} - y_j \right\|^2. \quad (7)$$

Here  $j^*$  is a function of  $(\mathbf{R}, \mathbf{t})$  and  $x_i$ . In general, Equation (7) can be implemented by KD-tree. When the correspondences in the point-sets are determined by Equation (7), Equation (6) can be used to recalculate  $\mathbf{R}$  and  $\mathbf{t}$ . For point-to-point registration problem, there is a closed-form solution for Equation (6) [41].

Given an initial transformation  $(\mathbf{R}, \mathbf{t})$ , ICP iteratively solves the problem by alternating between estimating the transformation with Equation (6), and finding closest-point matches with Equation (7).

**4.2. Global Optimal ICP for 2D Point-Set.** ICP is a typical nonconvex optimization problem. Therefore, it can only ensure that the algorithm converges to the local optimum. For this, Go-ICP uses BnB to achieve global optimal registration for 3D point-set [36]. Inspired by this, we attempt to promote this scheme to a 2D space to acquire global optimal registration for the 2D point-sets  $X$  and  $Y$ .

**4.2.1. BnB for 2D Point-Set Registration.** When using BnB, we need to determine the feasible range of parameters and the upper and lower bounds of  $E$ . Once a local optimal solution for  $\mathbf{R}$  and  $\mathbf{t}$  through ICP is acquired, BnB with given parameter range and bounds will help the algorithm to find a new solution with smaller error. In the following text, we will derive these two elements in 2D space.

**(1) Feasible Range of the Parameters.** For the rigid registration problem of 2D point-sets, the parameters involved include rotation matrix  $\mathbf{R}$  and translation vector  $\mathbf{t}$ . There are a total of six parameters in  $\mathbf{R}$  and  $\mathbf{t}$ .  $\mathbf{R}$  denotes a matrix with the size of  $2 \times 2$ , and  $\mathbf{t}$  denotes a vector of  $1 \times 2$ .

For convenience, we convert  $\mathbf{R}$  to angle-axis representation [42] as follows:

$$\mathbf{R} = \exp([\mathbf{r}]_{\times}) = I + \frac{[\mathbf{r}]_{\times} \sin \|\mathbf{r}\|}{\|\mathbf{r}\|} + \frac{[\mathbf{r}]_{\times}^2 (1 - \cos \|\mathbf{r}\|)}{\|\mathbf{r}\|^2}. \quad (8)$$

In Equation (8),

$$[\mathbf{r}]_{\times} = \begin{bmatrix} 0 & r \\ -r & 0 \end{bmatrix}. \quad (9)$$

In the following, we denote the rotation matrix corresponding to  $r$  as  $\mathbf{R}_r$ .

In this way, the number of parameters representing rotation and translation can be reduced to 3, they are one rotation angle and two translation parameters.

Obviously, the feasible region of  $r$  can be  $[-\pi, \pi]$ . For  $\mathbf{t}$ , we define its feasible region within a square  $[-\theta, \theta]^2$ , where  $\theta$  can be taken a relatively larger value.

(2) *The Upper and Lower Bounds.* It is easy to determine the upper bound of  $E$ , which is shown as Equation (10).

$$\bar{E} = \sum_{i=1}^m e_i(\mathbf{R}_{r_0}, \mathbf{t}_0)^2. \quad (10)$$

In Equation (10),  $\mathbf{R}_{r_0}$  and  $\mathbf{t}_0$  denotes the initial value of  $\mathbf{R}_r$  and  $\mathbf{t}$ . This means that the maximum  $E$  cannot exceed the result calculated from the initial values of  $\mathbf{R}_r$  and  $\mathbf{t}$ .

The lower bound of  $E$  can be defined as follows:

$$\underline{E} = \sum_{i=1}^m \max(e_i(\mathbf{R}_{r_0}, \mathbf{t}_0) - (\gamma_r + \gamma_t), 0). \quad (11)$$

In Equation (11),

$$\gamma_r = 2\sin\left(\min\left(\frac{\sigma_r}{2}, \frac{\pi}{2}\right)\right)\|\mathbf{x}_i\|, \quad (12)$$

$$\gamma_t = \sqrt{2}\sigma_t. \quad (13)$$

In Equations (12) and (13),  $\sigma_r$  and  $\sigma_t$  denote uncertainty radius of rotation and translation, respectively. They are the parameters that need to be assigned in the algorithm.

The specific derivation process of Equation (11) can be referred to Go-ICP. To further simplify the calculation, Go-ICP adopts a nested BnB strategy. In the strategy, an outer BnB searches the rotation and solves the bounds and corresponding optimal translations by calling an inner translation BnB.

**4.2.2. Hybrid ICP and BnB.** The specific algorithm process can be referenced to Go-ICP. Its basic idea is as follows:

Every time BnB searches for a solution with an upper bound of error smaller than the current one in the parameter branch, we implement ICP using  $r$  and  $\mathbf{t}$  corresponding to this solution. ICP and BnB are implemented collaboratively until the error function is small enough. Figure 4 vividly depicts this process.

**4.2.3. The Difference between the Proposed Method and Go-ICP.** The main technological process of the proposed method is similar to that of Go-ICP. However, Go-ICP is used to solve the registration problem in 3D space, and the proposed method is designed to tackle the rail profile registration problem in 2D planar. Therefore, the quantity, feasible regions, and boundaries of the parameters in the proposed method are all different from those of Go-ICP, which are described in Section 4.2.1. Specifically, there are six parameters include three rotations and three translations in Go-ICP, but only three parameters with one rotation and two translations in the proposed method. Due to fewer parameters involved in the operation, the operation speed will greatly increase. This is more suitable for high-speed dynamic measurement of the rail profile.

In addition, different from the oc-tree data structure in Go-ICP for rotation and translation, the rotation in our

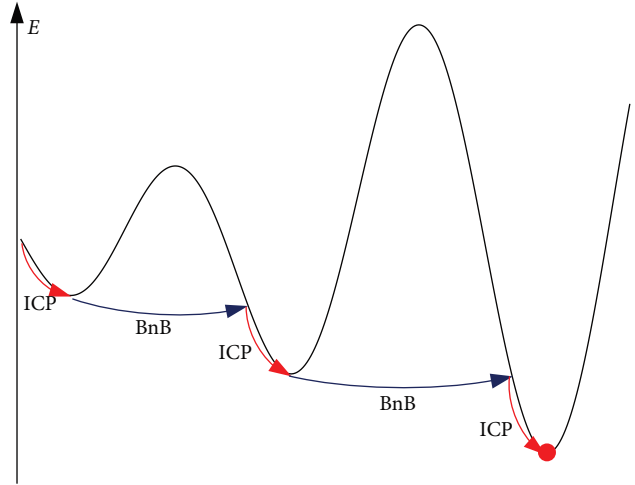


FIGURE 4: BnB and ICP collaboratively update the upper bounds of  $E$ .

method uses a binary tree, and the translation uses a quad-tree. Because rotation has only one parameter, each branch of  $r$  has two subbranches. Translation has two parameters, so each branch of  $\mathbf{t}$  has four subbranches. This also contributes to relieving computational burden.

**4.3. Sparse Sampling.** According to the analysis in Section 4.2, this algorithm needs to calls to BnB and ICP to process the point-set repeatedly. Generally, the quantity of the points in the point-set directly determines the calculation speed of the algorithm.

The dynamic measurement of rail profile requires fast algorithm speed, so we sample point-set sparsely before registration. In this section, we will try to compress the number of points in the set as much as possible while preserving the geometric features of the profile.

We use discrete curvature norm [43] to sample the points in the set. The result of this method is that areas with evident geometric changes retain more points, while areas with gentle changes in geometric features retain fewer points.

We select point  $\mathbf{x}_i$  and its nearby point  $\mathbf{x}_j$  separated by  $K$  points on the profile point-set, and  $\mathbf{n}_i$  and  $\mathbf{n}_j$  denote the normal vector at point  $\mathbf{x}_i$  and  $\mathbf{x}_j$ . Then we calculate the angle between these two normal vectors according to Equation (14) as follows:

$$\theta_i = \arccos\left(\frac{\mathbf{n}_i \cdot \mathbf{n}_j}{|\mathbf{n}_i||\mathbf{n}_j|}\right). \quad (14)$$

Setting a threshold  $\theta_T$ , and if

$$\theta_i > \theta_T, \quad (15)$$

we define the area between  $\mathbf{x}_i$  and  $\mathbf{x}_j$  as a dense sampling area, or define it as nondense sampling area. The sampling-ratio is higher in the dense sampling areas, while it is lower in the nondense sampling areas.



```

Input: 2D point-set  $X$  and  $Y$ 
Output: Optimal rotation and translation  $(\mathbf{R}^*, \mathbf{t}^*)$ ;
Initialization:  $(\mathbf{R}, \mathbf{t}) \leftarrow (\mathbf{R}_0, \mathbf{t}_0)$ ,  $\epsilon \rightarrow 0$ , and the other parameters;
Step1: Sparse sampling for  $X$  and  $Y$ 
Step2: Implement ICP, update  $(\mathbf{R}, \mathbf{t})$ , and calculate  $E$ 
  if
     $E < \epsilon$ 
    goto Step4
  else
    goto Step3
Step3: Implement BnB, update  $(\mathbf{R}, \mathbf{t})$ , and calculate  $E$ 
  if
     $E < \epsilon$ 
    goto Step4
  else
    goto Step2
Step4: End.

```

ALGORITHM 1: Fast global optimal ICP algorithm to 2D-point-set

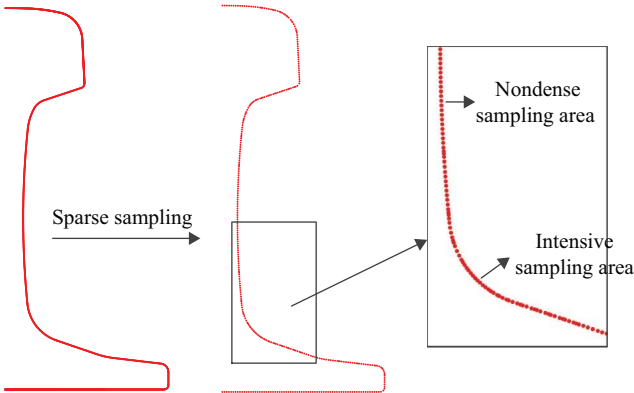


FIGURE 5: Sparse sampling for the rail profile point-set.

The sparse sampling result for the rail profile point-set is shown in Figure 5. We see that by sparse sampling, there are fewer points in the point-set, but geometric features are well-preserved.

**4.4. Algorithm Description.** In this section, we provide a brief description to the proposed fast global optimal ICP algorithm to 2D-point-set, which is shown in Algorithm 1.

Firstly, we initialize the parameters. In this step, we will set the initial values for rotation and translation, and set other parameters. Then, we sparsely sample rail profile point-set using the method in Section 4.3. Finally, we use the method in Section 4.2 for registration.

## 5. Experiments and Discussion

In this section, we validated the precision, stability, and efficiency of the proposed method through experiments. The experimental environments and devices are shown in Figure 6.

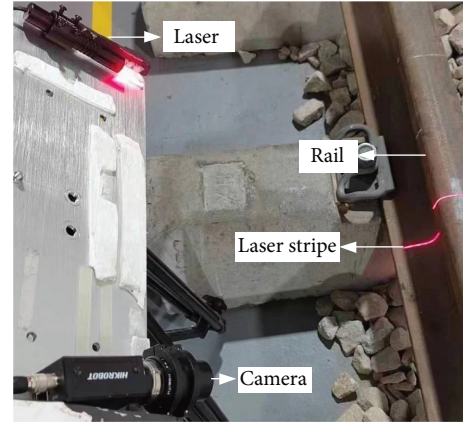


FIGURE 6: Experimental environments and devices.

TABLE 1: Parameters of the devices.

Device	Type	Main parameters
Laser	DS1235	Wavelength: 635–650 nm Straightness: <0.3% work distance: <500 mm
Camera	MV-CA004-10UM	Sensors: CMOS, IMX287 FPs: 526.5 Single pixel size: $6.9 \times 6.9 \mu\text{m}$ Resolution ratio: $720 \times 540$
Rail	–	60 kg/m

As shown in the Figure 6, the experiment is conducted on a track built in the laboratory. The main devices involved in the experiment include a camera, a laser, and a section of rail. The rail in the experiment is new and has no wear.

All the rail profiles in the following experiments are acquired by these devices; the main parameters of them are listed in Table 1.

**5.1. Precision and Stability Comparison Experiment.** In this section, we analyzed the precision and stability of our method. To verify the superiority, we tested the precision of similar registration algorithm include ICP [11] and RSICP [44]. In addition, we attempt to apply typical natural-inspired algorithms to ICP and compare them with our method. The nature-inspired optimization algorithms used for comparison include classical simulated annealing (SA) [30] and the recent algorithm called coati optimization (CO) [33]. We name them SA-ICP and CO-ICP, respectively.

The rail profile for this experiment was acquired statically. Besides, we employ Euclidean distance between the correspondences to visualize the registration error of the correspondence to verify the performance of these methods.

The comparison results of ICP, RSICP, SA-ICP, CO-ICP, and the proposed method are shown in Figure 7. Apparently, the traditional ICP cannot accurately register the two profiles. As shown in Figure 7(a), the maximum deviation is 4.983 mm because the traditional ICP can only converge to local optima. Once the initial value is inappropriate, it can lead to significant registration errors.

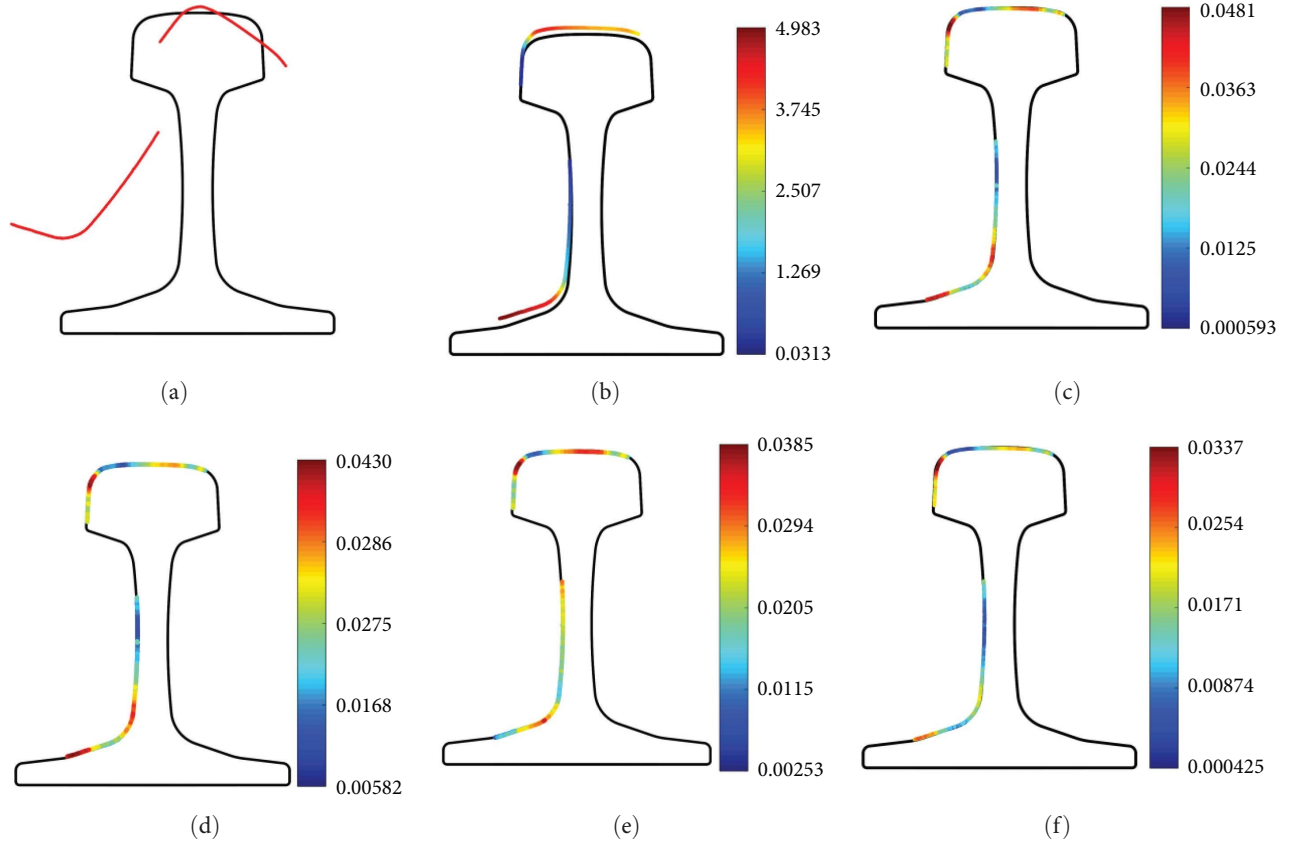


FIGURE 7: Comparison of the proposed method with other methods (unit: mm): (a) original position, (b) ICP, (c) RSICP, (d) SA-ICP, (e) CO-ICP, and (f) the proposed method.

TABLE 2: RMSE of ICP, RSICP, SA-ICP, CO-ICP, and the proposed method.

Method	RMSE (mm)
ICP	2.0736
RSICP	0.0277
SA-ICP	0.0231
CO-ICP	0.0205
Proposed	0.0182

TABLE 3: RMSE of the ICP, RSICP, SA-ICP, CO-ICP, and the proposed method under the influence of different levels of noise.

Method	RMSE (mm)		
	$\sigma = 0.003$	$\sigma = 0.005$	$\sigma = 0.01$
ICP	2.673	3.865	5.862
RSICP	0.0483	0.112	0.495
SA-ICP	0.0455	0.158	0.544
CO-ICP	0.0389	0.149	0.322
Proposed	0.0252	0.095	0.154

As shown in Figure 7(c)–7(e), RSICP, SA-ICP, and CO-ICP have improved registration accuracy to a certain extent. Our method solves the local minimum problem during the registration process. Regardless of the initial position, it always

TABLE 4: Comparison of the runtime, memory consumption and CPU cost of the ICP, RSICP, SA-ICP, CO-ICP, and the proposed method.

Method	Runtime (ms)	Memory (kB)	CPU (%)
ICP	12.3	972	12.5
RSICP	17.7	1,080	12.5
SA-ICP	632.58	2,880	12.5
CO-ICP	965.27	2,880	12.5
proposed	25.8	1,440	12.5

TABLE 5: Sampling rate settings.

No.	Sampling ratio (%)	
	Dense sampling areas	Nondense sampling areas
1	100	100
2	80	50
3	70	45
4	60	40

converges to the global optimum. Consequently, the precision is improved. In Figure 7(f), the maximum deviation is 0.0337 mm, which is more accurate than that of RSICP, SA-ICP, and CO-ICP.

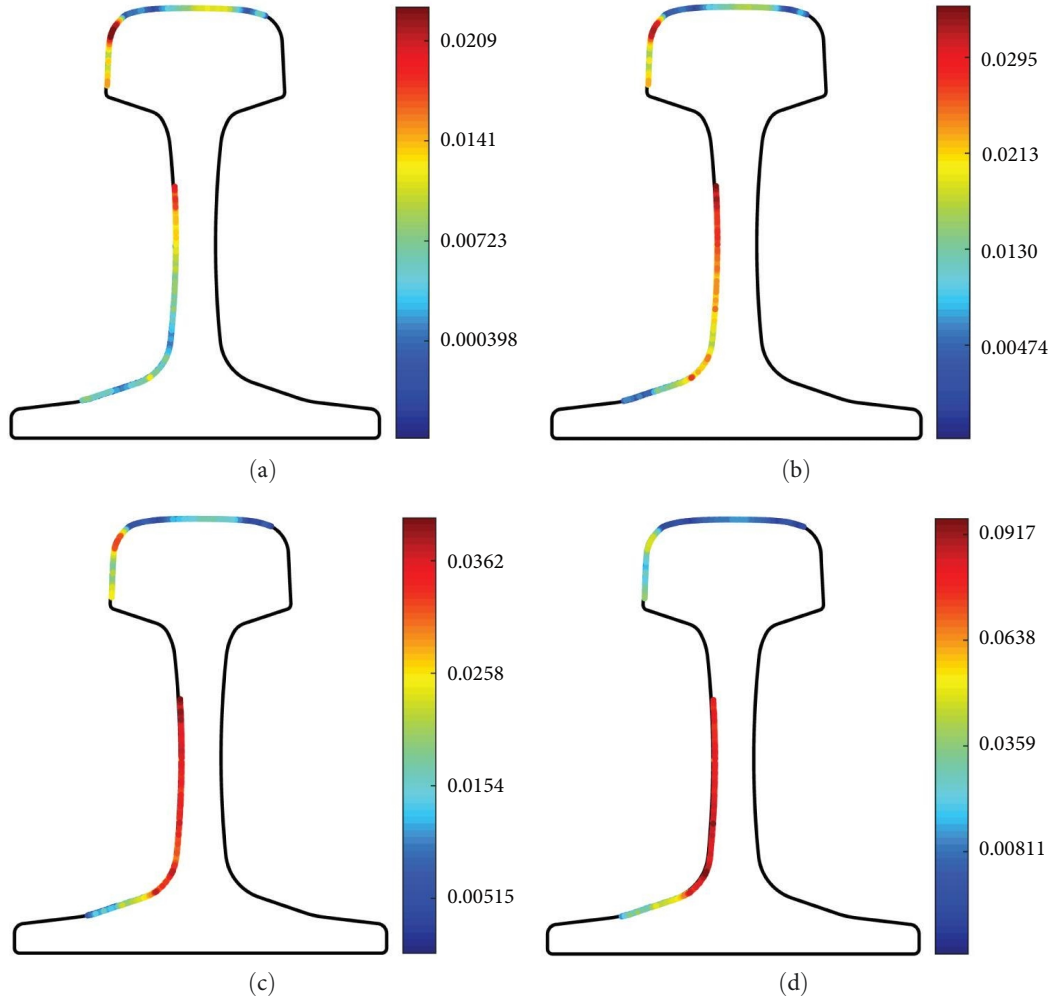


FIGURE 8: The registration deviation of our method under different sampling ratios (unit: mm): (a) ratio No. 1, (b) ratio No. 2, (c) ratio No. 3, and (d) ratio No. 4.

TABLE 6: The RMSE of our method under different sampling ratios.

No. of sampling ratio	RMSE (mm)
1	0.0122
2	0.0155
3	0.0194
4	0.0588

Table 2 shows the root-mean-square error (RMSE) of these three registration results. Evidently, the RMSE of the proposed is less than that of other methods.

To compare the stability of the proposed method and other algorithms, we added Gaussian random noise to the acquired rail profile to simulate the vibration during measurement. Then, we registered the noisy profile onto the standard profile by these five methods to verify the stability of them.

Table 3 shows the RMSE of these registration results under different noise levels. Similarly, under the same noise level, the RMSE of our method is less than that of others under noise.

TABLE 7: Time consumption of our method under different sampling ratios.

No. of sampling ratio	Runtime (ms)
1	136.2
2	65.8
3	26.5
4	22.1

**5.2. Efficiency Comparison Experiment.** The proposed method is implemented in the Visual Studio 2019. All the codes are programmed by C++ and examples were run on a personal computer with Intel i7 3.6 GHz CPU and 16 GB RAM. The sampling ratio of dense sampling areas is set to be 70%, and that of nondense areas is set to be 45%. In addition, we tested ICP, RSICP, SA-ICP, and CO-ICP under the same condition for comparison.

In this experiment, we used the above five methods to register 10 rail profiles, respectively. Table 4 shows the average runtime, memory consumption, and CPU cost of these three methods. The results indicate that the proposed method has



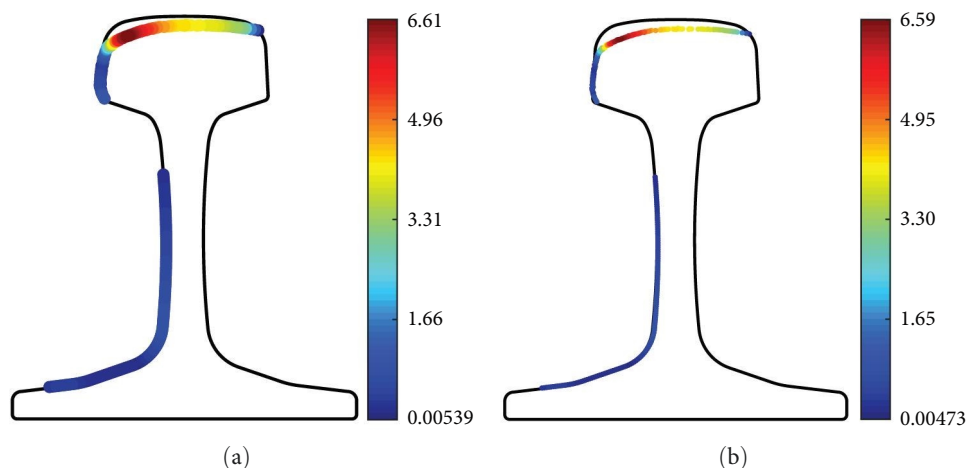


FIGURE 9: Comparison results of the proposed method and the Calipri (unit: mm): (a) Calipri and (b) the proposed method.

similar memory consumption and CPU cost to other methods. Besides, the convergence speed of our method is only a few milliseconds slower than ICP and RSICP, but apparently faster than that of SA-ICP and CO-ICP.

This indicates that our method satisfies the requirements of dynamic measurement for the rail. In a word, our method is not only highly precise but also highly efficient.

### 5.3. The Influence of Sampling Ratio on Efficiency and Precision.

In the Section 4.3, we know that the quantity of points in the point-set directly affects the calculation speed. Evidently, the more points, the lower the computational efficiency is. In this section, we quantitatively discussed the influence of sampling rate on the precision and efficiency for registration. For this, we tested the precision and time consumption of rail profile registration under for different sampling ratio. The four different sampling ratios are shown in Table 5.

Figure 8 shows the registration deviation of our method under the different sampling ratios. Overall, the lower the sampling ratio, the worse the registration precision will be. When the sampling ratio of dense sampling areas is lower than 60% and the sampling ratio of dense sampling areas is lower than 40%, the registration precision will be gradually decreased until it cannot satisfy the requirements of rail profile measurement.

Table 6 shows the RMSE of our method under the different sampling ratios, we see that when the sampling rate is too low, the registration error will also increase evidently.

Table 7 shows the time consumption of our method under different sampling ratios, we see that the lower the sampling ratio, the faster the algorithm speed will be. In a word, the sampling ratio is positively correlated with precision but negatively correlated with efficiency. In actual measurement, we need to set appropriate sampling ratio to balance the precision and efficiency.

**5.4. Application of Rail Wear Measurement.** In this section, we have conducted the dynamic measurement of rail wear along the Beijing–Jiulong line in China to verify the effectiveness of the proposed method in the actual situations.

Figure 9 shows the measurement results of a severely worn-out rail section. We compared the precision of our method with that of the Calipri [44], which a commonly used instrument in static track inspection. It can be observed that the measurement results of the two methods are quite close. Compared with the result measured by Calipri, Figure 9(b) indicates that the precision of our dynamic method is as precise as the industry instrumentation. Therefore, it can be concluded that the proposed method is suitable for the dynamic measurement of rail wear under actual environment.

## 6. Conclusion and Future Works

In this paper, we have proposed a fast global optimal registration method to 2D-point set, and applied it to the rail profile registration. The main works we have done in this paper are as follows:

- (1) We defined the feasible region and the upper and lower bounds of rotation and translation parameters in the error function in  $SO(2)$  space. Then we promote Go-ICP to 2D space to realize global optimal registration of 2D-point-sets.
- (2) Considering the strict real-time requirements in dynamic measurement of the rail profile, we sparse sampled the point-set before registration. This scheme improves the efficiency of the algorithm evidently.
- (3) Extensive experiments indicated that our method does not need too much computational cost but can keep stable measurement performance.

Although sparse sampling improves the efficiency of the proposed method, experiments have shown that this strategy comes at the cost of reducing precision. In the future, we intend to seek a fast global optimal registration algorithm without sparse sampling the original point-set.

## Data Availability

Data for this research article will be made available on a reasonable request.

## Conflicts of Interest

All authors declared no potential conflicts of interest with respect to the research, authorship, or publication of this article.

## Acknowledgments

This work is supported by the Key Laboratory of Intelligent Computing and Information Processing of Ministry of Education (No. 2022ICIP03), General Project of Hunan Provincial Department of Education (No. 23C0040), National Natural Science Foundation of China (No. 62103348), and Key Program of Hunan Provincial Department of Education (No. 22A0127).

## References

- [1] Y. Tang, F. Zhu, and Y. Chen, "For more reliable aviation navigation: improving the existing assessment of airport electromagnetic environment," *IEEE Instrumentation and Measurement Magazine*, vol. 24, no. 4, pp. 104–112, 2021.
- [2] N. Wang, H. Wang, S. Wang, X. Zhao, F. Wang, and J. Hao, "Research on calibration method of rail profile measurement system," *Journal of Circuits, Systems and Computers*, vol. 32, no. 10, Article ID 2350173, 2023.
- [3] J. Ye, E. Stewart, D. Zhang, Q. Chen, K. Thangaraj, and C. Roberts, "Integration of multiple sensors for noncontact rail profile measurement and inspection," *IEEE Transactions on Instrumentation and Measurement*, vol. 70, pp. 1–12, 2021.
- [4] P. Zhang, J. Moraal, and Z. Li, "Design, calibration and validation of a wheel–rail contact force measurement system in V-Track," *Measurement*, vol. 175, Article ID 109105, 2021.
- [5] S. Wang, H. Wang, Y. Zhou et al., "Automatic laser profile recognition and fast tracking for structured light measurement using deep learning and template matching," *Measurement*, vol. 169, Article ID 108362, 2021.
- [6] C. Wang and J. Zeng, "Combination-chord measurement of rail corrugation using triple-line structured-light vision: rectification and optimization," *IEEE Transactions on Intelligent Transportation Systems*, vol. 22, no. 11, pp. 7256–7265, 2021.
- [7] Y. Yang, L. Liu, M. Li, G. Yang, and B. Yi, "Sparse scaling iterative closest point for rail profile inspection," *Journal of Computing and Information Science in Engineering*, vol. 20, no. 1, Article ID 011003, 2020.
- [8] Y. Li, Y. Fu, K. Zhong, B. Ma, and Z. Yan, "A virtual binocular line-structured light measurement method based on a plane mirror," *Optics Communications*, vol. 510, Article ID 127974, 2022.
- [9] Y. Li, X. Zhong, Z. Ma, and H. Liu, "The outlier and integrity detection of rail profile based on profile registration," *IEEE Transactions on Intelligent Transportation Systems*, vol. 21, no. 3, pp. 1074–1085, 2020.
- [10] H. Gao, G. Xu, Z. Zhang, W. Zhou, and Q. Wu, "A novel probability iterative closest point with normal vector algorithm for robust rail profile registration," *Optik*, vol. 243, Article ID 166936, 2021.
- [11] P. J. Besl and N. D. McKay, "A method for registration of 3-D shapes," *IEEE Transactions on Pattern Analysis and Machine Intelligence*, vol. 14, no. 2, pp. 239–256, 1992.
- [12] H. Xie, Y. Zhang, J. Qiu et al., "Semantics lead all: towards unified image registration and fusion from a semantic perspective," *Information Fusion*, vol. 98, Article ID 101835, 2023.
- [13] H. Zhu, B. Guo, K. Zou et al., "A review of point set registration: from pairwise registration to groupwise registration," *Sensors*, vol. 19, no. 5, Article ID 1191, 2019.
- [14] Y. He, J. Yang, X. Hou, S. Pang, and J. Chen, "ICP registration with DCA descriptor for 3D point clouds," *Optics Express*, vol. 29, no. 13, pp. 20423–20439, 2021.
- [15] Y.-K. Yu, J.-M. Koo, M.-S. Oh, and I.-D. Yang, "Rail profile matching method using ICP algorithm," *The Transactions of The Korean Institute of Electrical Engineers*, vol. 65, no. 5, pp. 888–894, 2016.
- [16] S. Du, N. Zheng, L. Xiong, S. Ying, and J. Xue, "Scaling iterative closest point algorithm for registration of m-D point sets," *Journal of Visual Communication and Image Representation*, vol. 21, no. 5–6, pp. 442–452, 2010.
- [17] Z. Xiong, Q. Li, Q. Mao, and Q. Zou, "A 3D laser profiling system for rail surface defect detection," *Sensors*, vol. 17, no. 8, Article ID 1791, 2017.
- [18] B. Yi, Y. Yang, Q. Yi, W. Dai, and X. Li, "Novel method for rail wear inspection based on the sparse iterative closest point method," *Measurement Science and Technology*, vol. 28, no. 12, Article ID 125201, 2017.
- [19] H. Shi, Z. Zhang, and F. Li, "Study on automatic registration of rail profile during dynamic measurement of rail wear," *Journal of the China Railway Society*, no. 10, pp. 84–90, (in Chinese), 2021.
- [20] H. Yang, C. Gong, K. Huang, K. Song, and Z. Yin, "Weighted feature histogram of multi-scale local patch using multi-bit binary descriptor for face recognition," *IEEE Transactions on Image Processing*, vol. 30, pp. 3858–3871, 2021.
- [21] C. Zhu, J. Y. Yang, Z. P. Shao, and C. P. Liu, "Vision based hand gesture recognition using 3d shape context," *IEEE/CAA Journal of Automatica Sinica*, vol. 8, no. 9, pp. 1600–1613, 2021.
- [22] J. Ma, J. Zhao, J. Jiang, H. Zhou, and X. Guo, "Locality preserving matching," *International Journal of Computer Vision*, vol. 127, no. 5, pp. 512–531, 2019.
- [23] F. Shao, Z. Liu, and J. An, "Feature matching based on minimum relative motion entropy for image registration," *IEEE Transactions on Geoscience and Remote Sensing*, vol. 60, pp. 1–12, 2022.
- [24] A. Kumar, M. Nadeem, and H. Banka, "Nature inspired optimization algorithms: a comprehensive overview," *Evolving Systems*, vol. 14, no. 1, pp. 141–156, 2023.
- [25] C. C. W. Chang, T. J. Ding, M. A. S. Bhuiyan, K. C. Chao, M. Ariannejad, and H. C. Yian, "Nature-inspired optimization algorithms in solving partial shading problems: a systematic review," *Archives of Computational Methods in Engineering*, vol. 30, no. 1, pp. 223–249, 2023.
- [26] X. Zhan, Y. Cai, H. Li, Y. Li, and P. He, "A point cloud registration algorithm based on normal vector and particle swarm optimization," *Measurement and Control*, vol. 53, no. 3–4, pp. 265–275, 2020.
- [27] H.-G. Ha, G. Han, S. Lee et al., "Robot–patient registration for optical tracker-free robotic fracture reduction surgery," *Computer Methods and Programs in Biomedicine*, vol. 228, Article ID 107239, 2023.

- [28] H. Lin, C. Chang, and S. Liang, "3D Pose estimation using genetic-based iterative closest point algorithm," *International Journal of Innovative Computing, Information and Control*, vol. 14, no. 2, pp. 537–547, 2018.
- [29] C. K. Chow, H. T. Tsui, and T. Lee, "Surface registration using a dynamic genetic algorithm," *Pattern Recognition*, vol. 37, no. 1, pp. 105–117, 2004.
- [30] J. Luck, C. Little, and W. Hoff, "Registration of range data using a hybrid simulated annealing and iterative closest point algorithm," in *IEEE International Conference on Robotics and Automation. Symposia Proceedings*, pp. 3739–3744, IEEE, San Francisco, CA, USA, 2000.
- [31] N. L. Tao and H. Hiroshi, "Global iterative closet point using nested annealing for initialization," *Procedia Computer Science*, vol. 60, pp. 381–390, 2015.
- [32] S. Vankayalapati, L. Pappula, and D. Ghosh, "Element thinning using discrete cat swarm optimization for 5G/6G applications," *Progress in Electromagnetics Research B*, vol. 101, pp. 119–135, 2023.
- [33] M. Dehghani, Z. Montazeri, E. Trojovská, and P. Trojovský, "Coati optimization algorithm: a new bio-inspired metaheuristic algorithm for solving optimization problems," *Knowledge-Based Systems*, vol. 259, Article ID 110011, 2023.
- [34] R. A. Carbonneau, G. Caporossi, and P. Hansen, "Extensions to the repetitive branch and bound algorithm for globally optimal clusterwise regression," *Computers & Operations Research*, vol. 39, no. 11, pp. 2748–2762, 2012.
- [35] S. Liu, M. Wang, N. Kong, and X. Hu, "An enhanced branch-and-bound algorithm for bilevel integer linear programming," *European Journal of Operational Research*, vol. 291, no. 2, pp. 661–679, 2021.
- [36] J. Yang, H. Li, D. Campbell, and Y. Jia, "Go-ICP: a globally optimal solution to 3D ICP point-set registration," *IEEE Transactions on Pattern Analysis and Machine Intelligence*, vol. 38, no. 11, pp. 2241–2254, 2016.
- [37] Y. Liu, C. Wang, Z. Song, and M. Wang, "Efficient global point cloud registration by matching rotation invariant features through translation search," in *Computer Vision—ECCV 2018*, V. Ferrari, M. Hebert, C. Sminchisescu, and Y. Weiss, Eds., vol. 11216 of *Lecture Notes in Computer Science*, Springer, Cham, 2018.
- [38] A. L. Pavlov, G. W. Ovchinnikov, D. Y. Derbyshev, D. Tsetsrukou, and I. V. Oseledets, "AA-ICP: iterative closest point with Anderson acceleration," in *IEEE International Conference on Robotics and Automation*, pp. 3407–3412, IEEE, Brisbane, QLD, Australia, 2018.
- [39] Z. Zhang, "A flexible new technique for camera calibration," *IEEE Transactions on Pattern Analysis and Machine Intelligence*, vol. 22, no. 11, pp. 1330–1334, 2000.
- [40] J. Sun, "Universal method for calibrating structured-light vision sensor on the spot," *Journal of Mechanical Engineering*, vol. 45, no. 3, pp. 174–177, 2009.
- [41] S. Umeyama, "Least-squares estimation of transformation parameters between two point patterns," *IEEE Transactions on Pattern Analysis and Machine Intelligence*, vol. 13, no. 4, pp. 376–380, 1991.
- [42] K. F. Ma, X. M. Cui, G. P. Huang, D. B. Yuan, and Q. K. Cai, "A solution for space resection based on angle-axis representation," *Applied Mechanics and Materials*, vol. 638–640, pp. 2123–2128, 2014.
- [43] S.-J. Kim, C.-H. Kim, and D. Levin, "Surface simplification using a discrete curvature norm," *Computers & Graphics*, vol. 26, no. 5, pp. 657–663, 2002.
- [44] Y. Yang, L. Liu, B. Yi, and F. Chen, "Dynamic inspection of a rail profile under affine distortion based on the reweighted-scaling iterative closest point method," *Measurement Science and Technology*, vol. 30, Article ID 115202, 2019.